

A Restoration Scheme for Spatial and Spectral Resolution of Panchromatic Image Using Convolutional Neural Network

Xin Jin¹, Ling Liu¹, Xiaoxuan Ren¹, Qian Jiang^{1*}, Shin-Jye Lee², Jun Zhang³, Shaowen Yao¹

Abstract—Remote sensing images are the product of information obtained by various sensors, and the higher the resolution of the image, the more information it contains. Therefore, improving the resolution of the remote sensing image is conducive to identify earth resources from the remote sensing image. We present a multiple branch panchromatic image resolution restoration network based on convolutional neural network to improve the spatial and spectral resolution of panchromatic image simultaneously, named MBPRR-Net. Specifically, we adopt multi-branch structure to extract abundant features, and utilize a feature channel mixing block to enhance the interaction of adjacent channels between features. Feature aggregation in our method is used to learn more effective features from each branch, then a cubic filter is utilized to enhance the aggregated features. After feature extraction, we use a recovery architecture to generate the final image. Moreover, we utilize image super-resolution to restore spatial resolution and image colorization to restore spectral resolution, so that we compare with some image colorization and super-resolution methods to verify the proposed method. Experiments show that the performance of our method is outstanding in terms of visual effects and objective evaluation metrics against some existing excellent image super-resolution and colorization methods.

Index Terms—deep learning, artificial neural network, multispectral image, panchromatic image, remote sensing image processing.

I. INTRODUCTION

REMOTE sensing images play an important role in environmental monitoring [1], earth resource census [2], agricultural production [3], disaster prevention and mitigation [4], urban planning and construction [5]. Some satellites, such as Quickbird, WorldView-II, III, IV, are equipped with panchromatic (PAN) cameras and multispectral (MS) cameras. PAN cameras can shoot PAN images. The band of PAN image refers to all visible light bands $0.38\text{--}0.76\mu\text{m}$, and PAN image is the mixed image with all these bands. The PAN image

has high spatial resolution, but because it is just a mixed-band image displayed as gray level, the spectral resolution is low. MS images taken by MS cameras can make up for the deficiency of PAN images in spectral information. Compared with PAN image, MS image has higher spectral resolution, but because of the limitation of physical devices, MS image has lower spatial resolution. The improvement of Remote sensing images' spatial and spectral resolution is conducive to interpret the remote sensing scenes, so as to better play the role of remote sensing images in earth resource acquisition [6], [7]. Considering the advantages of PAN image and MS image, we design a multiple branch PAN image resolution restoration network (named MBPRR-Net) to enlarge the size of PAN image and the number of channels, so as to improve the spatial and spectral resolution simultaneously. An example of our idea is shown in Fig. 1 (a), and Fig. 1 (b) is used for visual contrast.

The goal of image super-resolution is to generate a high-spatial-resolution (HSR) image from a low-spatial-resolution (LSR) image. Thus, image super-resolution can be used to restore the spatial resolution of PAN image. It plays an important role in computer vision to improve the spatial resolution of an image. Super-resolution is helpful for image compression, for example, we can use the small image to transmit or save, and use the large image to view, which can reduce the amount of data transferred and saved. In recent years, deep-learning has received widespread attention in the field of image processing, some image super-resolution methods which are based on deep-learning [8]–[13] have made great progress. Among many methods, SRCNN model [8] first introduces deep-learning into image super-resolution, which uses CNNs to achieve a transition between LSR and HSR images. Dong et al. presented FSRCNN [9] to enhance SRCNN, accelerate the inference speed of model, and improve the quality of the output images. Recently, there are many other methods to optimize the performance of image super-resolution from the perspective of the model. For example, Zhang et al. [10] introduces a channel attention mechanism. Jiang et al. [11] added the dense module to the network to generate multi-scale features, then fused the features and reconstructed HSR images using pixel-shuffle operations. Similarly, Mei et al. [12] improve the super-resolution effect by designing a module that used cross-scale features. Using mean square error (MSE) or mean absolute error (MAE) as the loss function in image super-resolution often produces fuzzy images. To avoid generating blurred images, Ledig et al. [13] first applies adversarial loss to image super-resolution, which greatly improves the

This study is supported by the National Natural Science Foundation of China (Nos. 62101481 and 62261060), Basic Research Project of Yunnan Province (Nos. 202201AT070112, 202301AW070007, 202201AU070033, 202301AU070210, and 202005AC160007), Major Scientific and Technological Project of Yunnan Province (No. 202202AD080002), and Yunnan University expert workstations under Grant (202305AF150078). (Xin Jin and Ling Liu contributed equally to this work, and Qian Jiang is the corresponding author)

1. Engineering Research Center of Cyberspace, Yunnan University, Kunming, 650000, China, and School of Software, Yunnan University, Kunming, 650000, China. (xinxin_jin@163.com; liuling@mail.ynu.edu.cn; 17221140@bjtu.edu.cn; jiangqian_1221@163.com; yaosw@ynu.edu.cn)

2. Institute of Technology Management, National Chiao Tung University, Hsinchu 30010, Taiwan. (camhero@gmail.com)

3. China Mobile Communications Group Yunnan Co., Ltd. Yunnan, Kunming, 650000, China (18214590842@139.com)

(The code is available at <https://github.com/jinxinhua/MBPRR-Net/>)

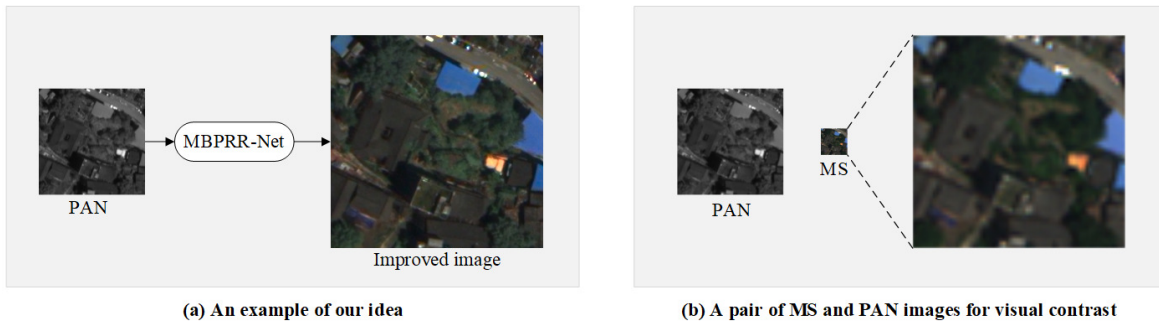


Fig. 1: An example of our idea for remote sensing image restoration.

reality of reconstructed images. However, there are still some problems with the above methods, such as it is difficult to express all the textures in the GANs, so in some places with complex textures will generate wrong textures.

The goal of image colorization is to generate a colorized image with three channels from a gray-scale image with one channel. In general, a color image (such as MS image) has more abundant spectral or color information than that of gray image (such as PAN image). Thus, image colorization can be used to restore the spectral resolution of PAN image. Conventional image colorization methods depend on user's guide, such as scribbles [14]–[16], reference images [17]–[19], and semantic information [20], [21]. User-guided colorization methods have limitations that require user interaction. It can improve the limitation of the user-guided colorization methods when using deep-learning. The gray-scale image colorization algorithm based on convolutional neural networks (CNNs) [22]–[25] belongs to supervised learning, and the label of image colorization training phase is color image. Generative adversarial networks (GANs) can be regarded as unsupervised learning networks, which consist of a generator and a discriminant. The parameter's update of the generator is guided by the discriminant. Therefore, GANs-based image colorization [26]–[29] can generate colorized images. Existing studies show that deep learning plays an important role in image colorization, but there are some limitations to these methods, such as it fails to solve multimodal problems [22], relies on color distribution [23] or object detection algorithm [25], needs amounts of data to train [26], etc. Therefore, image colorization is still a challenging problem and awaits further exploration.

Some existing methods combine pansharpening to improve the spectral resolution of PAN images. For instance, Ozcelik et al. [30] borrowed the idea of pansharpening to input PAN images and MS images into a guided colorization model to improve the spectral resolution of PAN images. Lu et al. [31] refer to hyper-sharpening and pansharpening techniques, while reconstructing the HSR image with a two-stage cascaded CNN. However, pansharpening methods usually need to input PAN images and MS images to the model at the same time, and do not involve the improvement of spatial resolution.

In this paper, we introduce a novel MBPRR-Net model to restore the spatial and spectral resolution of PAN image based on the characteristics of PAN image. First, there are large differences between the same class and small differences be-

tween different classes in a remote sensing, that is, the spectral information between objects of the same type is very different, and the spectral information between objects of different types are very close, which will lead to large deviation between the reconstructed spectral information and the true spectral information. To solve this problem, we consider to design a network which is powerful in feature extraction. Second, the PAN image has a complex background and many small objects, which will reduce the quality of the image when the spatial resolution is increased. We consider to use a feature enhancement method to solve this problem. Third, Due to the complementarity of PAN and MS images, we consider to use the original PAN image as the brightness label to improve the spatial resolution, and utilize MS image's chroma information as the chroma label to predict the spectral information.

The main contributions of this paper are shown as follows:

- We propose a multi-branch PAN image resolution restoration network (MBPRR-Net) to reconstruct an image with both high spatial and spectral resolution, and the MBPRR-Net only needs to input PAN image.
- We design a feature channel mixing block (FCMB) to enhance the channel correlation between features. Experiments show that FCMB can extract effective features and facilitate the feature recovery.
- We employ a cubic filter to enhance the extracted features to help the model generate a color image with clear texture, and also design a self-convolution blocks (SCB) to recovery the extracted features.
- We train our model to predict PAN image's spectral information according to MS image, so that the spectral resolution reconstruction result of PAN image is consistent with the real scene.

The rest of this paper is arranged as follows. Section II reviews some papers about image super-resolution and image colorization methods. Section III give an account of the proposed method. Section IV discusses the performance of our method. Section V makes a summary of this work.

II. RELATED WORK

This section gives a review of the existing image super-resolution and colorization methods, respectively.

A. Image Super-Resolution

Image super-resolution restores clear texture from a LSR image, and finally gets a HSR image. In recent years, thanks to the powerful learning ability of deep-learning technology, image super-resolution has made remarkable progress. LSR images are typically obtained through a series of degradation operations, which not only lose a lot of details, but also introduce a series of noise. In essence, the super-resolution process based on deep-learning belongs to a supervised learning which uses a pair of HSR and LSR images to train the network model, and then a inverse operation of the above degradation operation is used to reconstruct the HSR image.

Dong et al. [8] first applied CNNs to the image super-resolution technology, and achieved a great improvement in the quality of generated image compared with conventional interpolation and optimization algorithms. In particular, this method was further optimized by FSRCNN model [9], which greatly accelerated the speed of training. Ledig et al. [13] used GANs to solve the problem of super-resolution. They proposed that it could improve PSNR value when using MSE as the loss function in network training, but the details information of recovered images were lost usually. Therefore, Ledig et al. used perceptual loss and adversarial loss to improve the authenticity of the recovered images. Lim et al. [32] removed unnecessary modules from the conventional resnet [33] structure and improved the super-resolution reconstruction performance. To solve the problem of deep network is difficult to train, Zhang et al. [10] proposed a new structure named RCANs, it used a channel attention mechanism to give Channel-wise different attention, so as to increase the interdependence among channels. To improve the performance of super-resolution, some effective models, such as [10], [13], [32], are designed by increasing the complexity of the model. However, these methods still have problems with a large solution space, which leads to limit the performance of super-resolution and cannot produce satisfactory texture. To reduce solution space of mapping function between LSR and HSR, Guo et al. [34] proposed a network named DRN, which used a dual regression structure to improve the performance of the super-resolution model.

B. Image Colorization

1) *User-guided colorization*: Most of the early image colorization methods were guided, such as scribble-based colorization [14]–[16], example-based colorization [17]–[19], and text-based colorization [20], [21].

Scribble-based colorization. Scribble-based colorization methods need users to provide scribbles to guide the colorization process. For instance, Anagnostopoulos et al. [14] began with the user drawn abstract color indications, and then splashed multiple colors on the sketch to get the color image, at last, refined the color image to realize colorization. Ci et al. [16] and Sangkloy et al. [15] utilized GANs in scribble based hand-draw sketch colorization.

Example-based colorization. It is crucial to use appropriate reference images to realize example-based colorization methods. Reference images usually come from the user's [18],

[19] or the Internet [17]. Lee et al. [19] utilized the image with identical geometric distortion as a reference image, and then an attention mechanism are used to transfer color from the reference image to the sketch. To select reference image efficiently. He et al. [18] proposed the deep learning approach to predict colors from an aligned reference image to a gray-scale image directly. To avoid providing reference images from the user directly, Alex et al. [17] designed a colorization system that searched reference images on the Internet, the user was required to provide semantic text labels or semantic cues for searching reference images on the Internet.

Text-based colorization. To complete image colorization with the help of textual messages, text-based colorization method uses textual messages and images as the input. Bahng et al. [20] and Kim et al. [21] captured the semantics of the input to generate color information. There is a serious problem with these methods, that is, it is difficult to recognize the text semantics.

All of these methods need numerous user's interactions, and whether or not these methods can produce a realistic color image depends on the guidance provided by user. In brief, user-guided colorization methods have significant limitations.

2) *Fully automatic colorization*: Fully automatic colorization methods are proposed to address the limitations of user-guided colorization methods. Fully automatic colorization base on deep-learning has achieved great achievement. The existing deep-learning based colorization methods can be divided into two types: CNNs-based methods [22]–[25] and GANs-based methods [26]–[29].

CNNs-based colorization. Iizuka et al. [22] proposed an fully automatic colorization method to combine global information and local features. To address the multimodal problem, Zhang et al. [23] argued that image colorization task is a kind of classification task, and they rearranged class distribution during model training phase to increase the diversity of the color. Özbülak et al. [24] proposed designed a capsule network with generative and segmentation capabilities, this method is easy to cause the problem of color discontinuity between two adjacent small blocks. Su et al. [25] used a existing object detection algorithm to extract object of the input image, then used a color network to color object and full-image except object respectively, finally they fused object and full-image except object to generate the final colorized image.

GANs-based colorization. GANs-based image colorization methods mainly solve multimodal problems [28] and model training problems that require large amounts of data [27], [29]. CNNs require a lot of manual labor when designing effective loss functions, whereas GANs can automatically learn a loss function suitable for achieving the image colorization task. Isola et al. [26] designed a network to learn a mapping from the input image to the output image, at same time, they designed a loss function to optimize the mapping network to achieve image translation tasks involving the image colorization. Vitoria et al. [28] proposed an adversarial strategy to capture geometric, perceptual, and semantic information from input image, and they utilized these information to realize image colorization. To solve the problem that needs a lot of data to train, Yoo et al. [27] proposed a colorization model

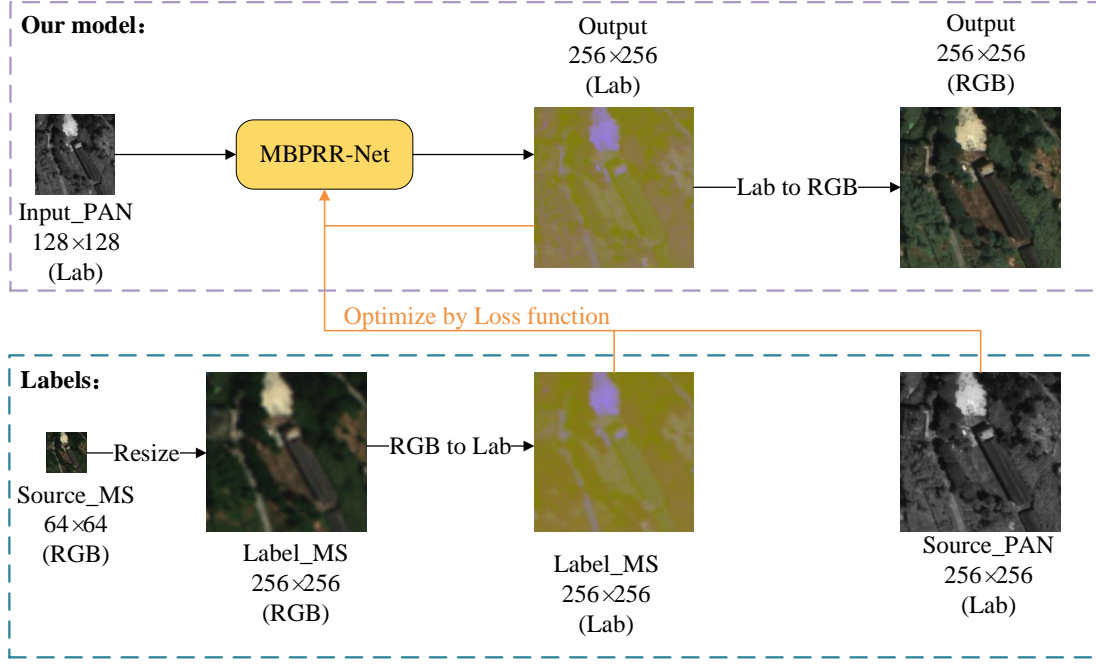


Fig. 2: The proposed framework of the PAN image spatial and spectral resolution restore.

which is added a memory-augmented unit to produce colorized images with a small amount of data. However, this model only focused on major color transfers and ignored minor color transfers. Since the pix2pix method is restricted by pairs of images, which may be difficult to obtain for SAR images, Ji et al. [29] used a multidomain cycle-consistency generative adversarial network for SAR image colorization which did not use pairs of images to train the model.

III. THE PROPOSED METHOD

To restore the spatial and spectral resolution of PAN image simultaneously, we introduce a new PAN image colorization and super-resolution model based on CNNs. In this method, VGG19 [35] is invoked as the backbone to extract image features. Moreover, multiple branches are applied to extract rich features. A feature aggregation module is proposed to further utilize the extracted features from various branches. Finally, we employ a feature recovery module to generate the colored and super-resolution images. Besides, we designed a loss function which is composed of $L1$ and structural similarity (SSIM) to measure the errors. The errors consists with two sets, the first set is the error between the source PAN image and the brightness channel of generated image, the second set is the error between the ab channels of the resized source MS image and the ab channels of the output image. In this section, we describe the detail of the proposed network structure, loss function, and parameters setting.

A. Proposed Framework

The proposed PAN image spatial and spectral restoration framework is shown in Fig. 2. Source images are pairs of gray PAN images and MS images with B ($B > 3$) spectral

bands. We denote PAN image as $S_{PAN} \in \mathbb{R}^{H \times W}$, MS images as $S_{MS} \in \mathbb{R}^{\frac{H}{scale} \times \frac{W}{scale} \times B}$. The MBPRR-Net model mainly including three modules: feature extraction module, feature aggregation module, and feature recovery module. The input of MBPRR-Net is the PAN image, to realize image super-resolution, we resize S_{PAN} to $X_{PAN} \in \mathbb{R}^{\frac{H}{2} \times \frac{W}{2}}$ as input image. The output of MBPRR-Net is the colorized HSR images in CIELab color space, we denote it as $\hat{Y}_{colored_Lab}$. To facilitate visual analysis, the color space of model output images will be converted from CIELab into RGB, we denote the output image in RGB color space as $\hat{Y}_{colored}$.

There are three considerations during the training phase that differ from the testing phase. First, we considered using MS images as the label of chrominance information to overcome the limitation of PAN images (lack of spectral information). Meanwhile, to achieve the separation of luminance information and chromaticity information, we convert the colorspace of MS image from RGB to CIELab because that L channel represents luminance information and ab channels represent chromaticity information in CIELab color space. Second, Because of PAN images have richer spatial details than MS images, we utilize source PAN images as the label of luminance information. Finally, due to source MS images' resolution are only a quarter of source PAN images, MS images must be resized to match the source PAN images. In a word, ab channels of resized MS images $Y_{MS} \in \mathbb{R}^{H \times W \times B}$ in CIELab color space $Y_{MS_Lab} \in \mathbb{R}^{H \times W \times B}$ is the label of $\hat{Y}_{colored_Lab}$'s ab channels, meanwhile, S_{PAN} is the label of $\hat{Y}_{colored_Lab}$'s L channel. All parameters can be automatically updated by minimizing the loss among the output of MBPRR-Net $\hat{Y}_{colored_Lab}$ and a pair of images (S_{PAN} and Y_{MS_Lab}). In short, our framework is represented as:

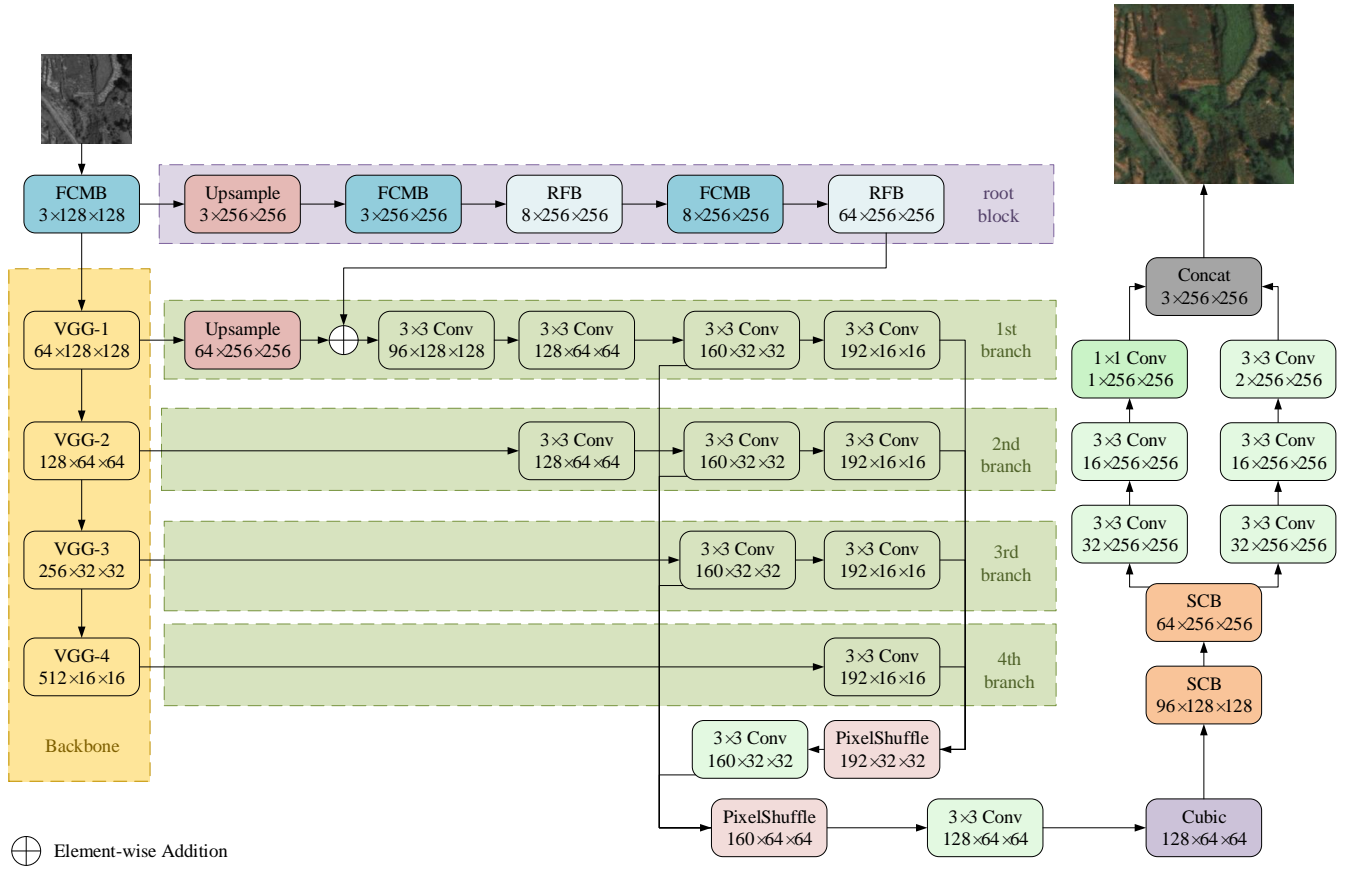


Fig. 3: The proposed MBPRR-Net model structure.

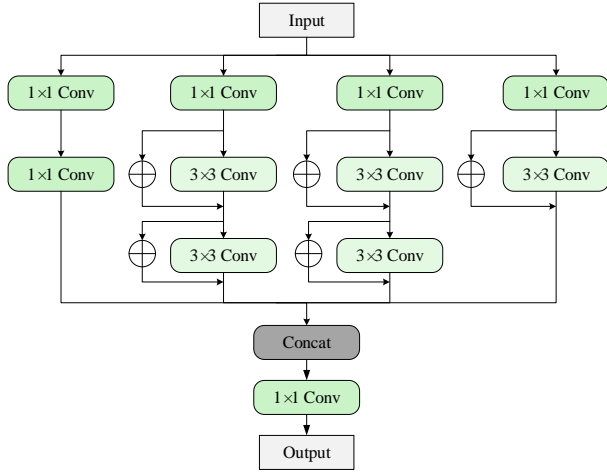


Fig. 4: RFB structure detail.

$$\hat{Y}_{colored_Lab} = \mathcal{M}(X_{PAN}), \quad (1)$$

where $\mathcal{M}(\cdot)$ is MBPRR-Net model.

B. Multiple Branch PAN-image Resolution Restoration Network

The architecture of our MBPRR-Net model is represented in Fig. 3. It makes up of feature extraction, feature aggregation,

and feature recovery. The overall network structure is inspired by the U-shape neural network, feature extraction module and feature aggregation module can be regarded as an encoder, feature recovery module can be seen as a decoder. First, we design a module to extract the features of PAN image. Then, we utilize a operation named pixel-shuffle to aggregate these extracted features. At last, we design a decoder to generate a new colorized HSR image that improve the spatial resolution of PAN image and learn the rich spectral information of MS image.

1) Feature Extraction Module: Inspired by [36], the feature extraction module uses VGG19 as a backbone block, and we only use the first 12 layers before the max-pooling layers and remove the last 7 layers of VGG19. In addition, there are four branches to get rich features. We extract features in different scales before each max-pooling layers of VGG19 and input to four branches respectively. The choice of the number of branches will be discussed later in the ablation study. In order to realize image super-resolution, a FCMB block is used at the beginning of this model, up-sample operations are used at the beginning of root branch and the first branch. Inspired by [37], we add Receptive Field Block (RFB) in the root block to expand the receptive field and improve feature extraction capability of the proposed network. RFB uses four branches to extract features of different scales. In each branch, 1×1 convolution is used to change the number of channels to

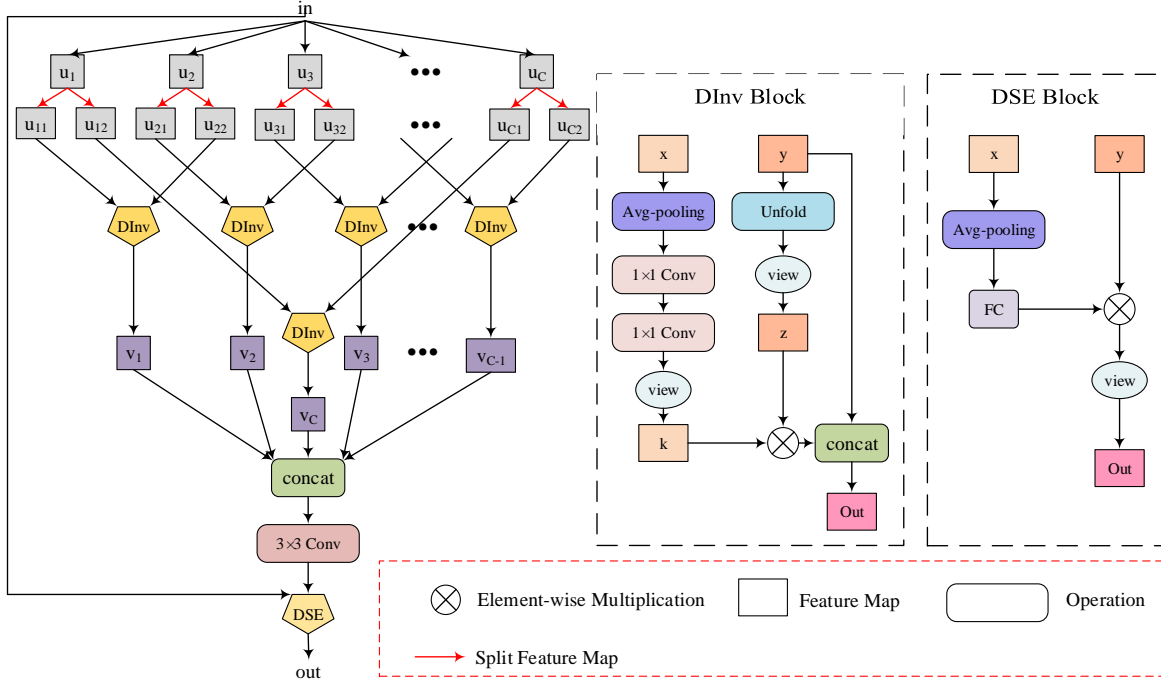


Fig. 5: The structure of feature channel mixing block (FCMB).

reduce the number of parameters. At the same time, a residual structure is used in each branch to prevent vanishing gradient problem. Fig. 4 has shown RFB structure. FCMB improves the interdependence between image channels by mixing features of different channels and adding attention between adjacent channels. Our FCMB diagram is displayed in Fig. 5. First, the input image is divided into C feature maps (C represents input image's channel number), these feature maps are denoted as u_i . Second, we split u_i in half to get u_{i1} and u_{i2} . Third, we use a dual-involution (DInv) block inspired by [38] to enhance the correlation between two adjacent channels, and generate a mixing feature map denoted as v_i . Fourth, we use a concat operation to combine all v_i features. Fifth, the combined features go through a convolution block, a Dual-Squeeze-and-Excitation (DSE) block inspired by [39] to get the output. We formulate the FCMB as:

$$v_i = \begin{cases} \mathcal{K}(I_{(i,1)}, I_{(i+1,2)}), & i \neq c; \\ \mathcal{K}(I_{(1,2)}, I_{(i,1)}), & i = c, \end{cases} \quad (2)$$

$$out_{(p,q)} = \mathcal{S}(\Phi(\mathcal{C}(v_1, v_2, \dots, v_c), W_{(p,q)}), X_{(p,q)}), \quad (3)$$

where $I_{(i,j)}$ represents the j -th part of the i -th channel of the input feature map, the value of i is from 1 to c (c is the input feature's channel number), the value of j is 1 or 2. $out_{(p,q)}$ is the value at point (p, q) on the output feature map of FCMB, $\mathcal{K}(\cdot)$ represents a dual-involution block, $W_{(p,q)}$ represents the convolution weight of pixel (p, q) , $X_{(p,q)}$ denotes the value at point (p, q) on the input feature map of FCMB, $\mathcal{C}(\cdot)$ is concat operation, $\Phi(\cdot)$ is convolution operation, $\mathcal{S}(\cdot)$ is the DSE block. Each branch finally gets a feature map of the same size to facilitate later feature aggregation.

2) *Feature Aggregation Module*: The proposed feature aggregation module consists of two pixel-shuffle blocks and a

cubic filter, which is inspired by [40]. First, we concatenate the last and penultimate features of each branch of the feature extraction module respectively. Second, these two concatenated features through a pixel-shuffle operation become two aggregated features, and then a convolution operation is used to produce a feature map with a specific number of channels. Finally, a cubic filter are utilized to improve the global connectivity of aggregated features. The graphical representation of cubic filter is shown in Fig. 6. We formulate the cubic filter as:

$$O(x, y) = C(I(x, y), Q(x, y)) \odot P(X, Y) \oplus I(x, y), \quad (4)$$

where \odot is a matrix dot product, and \oplus is a matrix addition. $O(x, y)$ is the value at pixel (x, y) on the output feature of cubic filter. $I(x, y)$ is the value at pixel (x, y) on the input feature of cubic filter. $Q(x, y)$ denotes the weight of filter for pixel (x, y) . $C(\cdot)$ is the Conv-Pool-FullConnection module which including three part, the first part is consists of three layers of alternating convolution and maxpooling operations, and followed by a convolutional layer to adjust the number of channels; the second part is a global average pooling layer to expand the feature into a vector; the finally part is a full-connection (FC) layer to adjust the vector size. $P(X, Y)$ is a polynomial from [40]. X is a $H \times H$ vandermonde matrix, and Y is a transpose of $W \times W$ vandermonde matrix. Since the output of FC is a vector but the output of $P(X, Y)$ is a matrix, we need to reconstruct the dimensions of FC's output to ensure that the output of FC and the output of P can carry out \odot operation.

3) *Feature Recovery Module*: The feature recovery module consists of two self-convolution blocks (SCB) and six convolution layers, which are used to generate the final colorized HSR

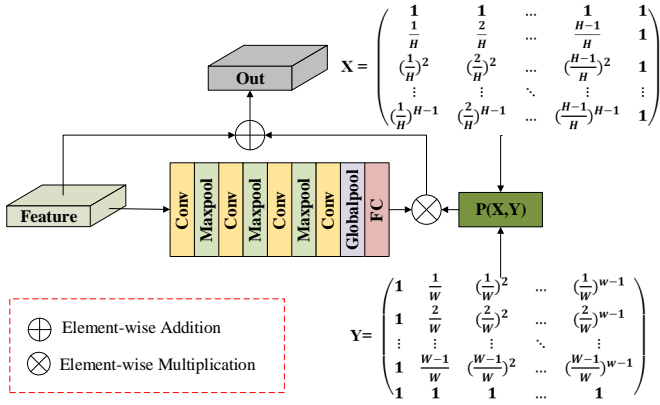


Fig. 6: The diagram of cubic filter.

image. First, we use SCB to adjust the size of the feature maps. SCB consists of two standard convolution layers, an involution [38] layer, and a pixel-shuffle layer. SCB utilizes the involution layer to reduce kernel redundancy on the channel. The standard convolution kernels have a remarkable property, that is the convolution kernels is shared in the spatial dimension, but independent in the channel dimension. Involution has the characteristic of symmetric inversion compare with standard convolution. In the feature recovery stage, enlarging the size of feature map is a key step, we utilize a pixel-shuffle layer in SCB to enlarge the size of feature map. Then, we divide six convolution layers into two groups to generate the L channel and ab channels of output image, respectively. Finally, we employ a concat operation to merge the L channel and ab channels and generate the image with high spatial and spectral resolution.

C. Loss Function

In this work, we adopt the \mathcal{L}_1 and SSIM as the final loss function, and it is formulated as follows:

$$\mathcal{L} = \alpha \mathcal{L}_1(\hat{Y}_{colored_L}, S_{PAN}) + \beta \mathcal{L}_1(\hat{Y}_{colored_ab}, Y_{MS_ab}) + \eta \text{SSIM}(\hat{Y}_{colored_Lab}, \mathcal{C}(S_{PAN}, Y_{MS_ab})), \quad (5)$$

where $\mathcal{L}_1(\cdot)$ represents the \mathcal{L}_1 loss and its formula refer to (6), $\text{SSIM}(\cdot)$ is the SSIM loss and its formula refer to (7). $\mathcal{C}(\cdot)$ is a concat operation, we use $\mathcal{C}(\cdot)$ to concatenate the original PAN image and the ab channels of Y_{MS_ab} to get a label image denoted Y_{label_Lab} with three channels in CIELab color space. $\hat{Y}_{colored_L}$ and $\hat{Y}_{colored_ab}$ are the L channel and ab channels of our MBPRR-Net model's output $\hat{Y}_{colored_Lab}$, respectively, Y_{MS_ab} is ab channels of the resized MS image. In this work, we calculate three-part loss, the first part is \mathcal{L}_1 loss between $\hat{Y}_{colored_L}$ and S_{PAN} , the second part is \mathcal{L}_1 loss between $\hat{Y}_{colored_ab}$ and Y_{MS_ab} , the third part is SSIM loss between $\hat{Y}_{colored_Lab}$ and Y_{label_Lab} . α , β and η are the weight of the above-mentioned three-part loss, we set α , β and η as 1.

$$\mathcal{L}_1(x_1, x_2) = \sum_{i=1}^n |x_1^{(i)} - x_2^{(i)}|, \quad (6)$$

$$\text{SSIM}(p, q) = [l(p, q)]^\rho [c(p, q)]^\tau [s(p, q)]^\varphi, \quad (7)$$

where SSIM is composed of three contrast modules: luminance contrast function $l(p, q)$, contrast contrast function $c(p, q)$, and structural contrast function $s(p, q)$.

D. Parameters setting

We present the key parameters setting of our proposed MBPRR-Net, including hyperparameters setting, model training and testing details.

All convolution layers use a convolution kernel of size 3×3 except the last convolution of SCB is 1×1 . We set the convolution stride of the feature extraction module as 2, and the rest of the modules as 1. We use a zero-padding strategy in all 3×3 convolution layers to keep the image size fixed. All activation functions in our module are using Mish function [41], the formula for the Mish function refer to (8).

$$\text{Mish}(x) = x \cdot \tanh(\ln(1 + e^x)). \quad (8)$$

TABLE I: Model training parameters setting.

Parameters	Name	Value
Input	degraded PAN image	128×128
Batchsize	-	6
Epoch	-	100
Learning rate	-	1×10^{-4}
Learning schedule	StepLR	adjust epoch
		reduction rate
		0.8

All model training parameters in Table I are remained the same in all experiments. We initialize the layers of backbone with the weights of the pre-trained VGG19 on ImageNet and randomly initialize the rest layers.

For model testing, we use three test strategies. The first one is that we input source PAN image into our trained MBPRR-Net directly, and the model output image's spatial resolution is 512×512 . The second one is that we degrade the source PAN images to 128×128 as input, and the model output image's spatial resolution is 256×256 . The last one is that we clip the source PAN image to 128×128 as input, and the model output image's spatial resolution is 256×256 . These strategies are used to demonstrate that our MBPRR-Net model can improve arbitrary size PAN images' spatial and spectral resolution, whether PAN images are degraded or not.

Both model training and testing of the proposed MBPRR-Net are implemented by using an NVIDIA GeForce GTX 2080Ti GPU based on PyTorch framework.

IV. EXPERIMENTS AND ANALYSIS

In this section, we use a lot of experimental analysis to verify the effectiveness of the MBPRR-Net model. First, the selection of datasets in our works is described. Second, the evaluation metrics are described. Third, our method is

compared with some representative image colorization and image super-resolution methods. Finally, some ablation studies are used to validate our model design selection.

A. Datasets

In this work, our images come from QuickBird satellite and WorldView-II satellite. The QuickBird dataset contains panchromatic images with spatial resolution of 0.61-0.72m and multispectral images with spatial resolution of 2.44-2.88m. The WorldView-II dataset contains panchromatic images with spatial resolution of 0.5m and multispectral images with spatial resolution of 1.8m. For a pair of PAN and MS images taken by one satellite in the same scene, the width and height of the MS image are both a quarter of the PAN image. Our training dataset has 2800 pairs of PAN images and MS images, including 1400 paired images from QuickBird and 1400 paired images from WorldView-II, and the test dataset has 240 pairs of PAN images and MS images, including 120 paired images from QuickBird and 120 paired images from WorldView-II.

The selection of dataset includes three steps. First, we select PAN images and the corresponding MS images from QuickBird or WorldView-II. Second, we clip PAN and MS images into small image patches in which the size of PAN image patch is 256×256 and MS image patch is 64×64 . Finally, we randomly shuffle image patches and then select PAN and MS image pairs as training set or a test set.

B. Evaluation Metrics

We utilize a variety of image quality evaluation metrics to conduct objective analysis of the MBPRR-Net model's output images, including Peak Signal-to-Noise Ratio (PSNR), Cross Correlation (CC), Universal Image Quality Index (UIQI), Spectral Angle Mapper (SAM). The higher metrics represent the better the image quality except SAM. In this section, we denote the image generated by our MBPRR-Net model as $\hat{Y} \in \mathbb{R}^{C \times H \times W}$, label image is expressed as $Y \in \mathbb{R}^{C \times H \times W}$, \hat{y}_j and y_j denote the j th columns of \hat{Y} and Y , respectively. \hat{y}^i and y^i denote the i th bands of \hat{Y} and Y , respectively.

1) *MSE*: MSE is the average of the square of the error between true image x_1 and processed image x_2 that can be calculated as follows:

$$\text{MSE} = \frac{1}{n} \sum_{i=1}^n (x_1^{(i)} - x_2^{(i)})^2, \quad (9)$$

2) *PSNR*: PSNR is the logarithm of the highest pixel value of the processed image x_2 divided by the MSE of the true image x_1 and the processed image x_2 , PSNR is formulated as follows:

$$\text{PSNR} = 10 \times \lg\left(\frac{\text{MAX}_{x_2}^2}{\text{MSE}(x_1, x_2)}\right), \quad (10)$$

where $\text{MAX}_{x_2}^2$ represents the maximum pixel value of x_2 , $\text{MSE}(\cdot)$ is calculated by equation (9). The higher the PSNR value of the processed image, the better the processing effect of the image (the lower the distortion of the image). Note that the unit of PSNR is dB.

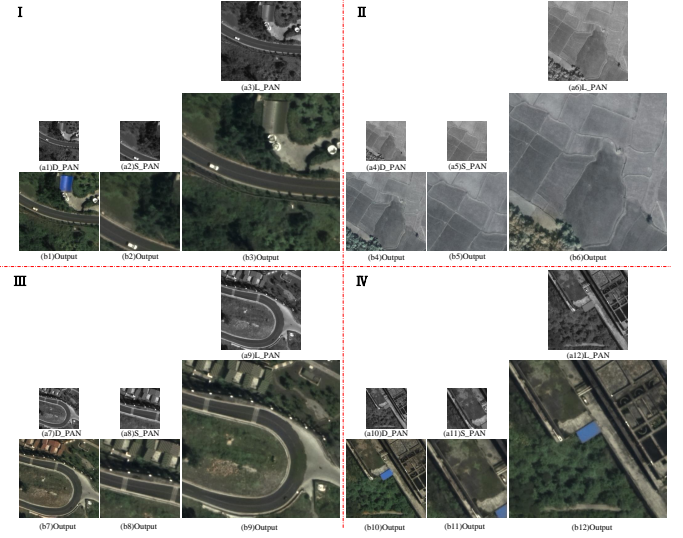


Fig. 7: Some results of our MBPRR-Net when inputting images of different sizes. (a) Inputs, $D_PAN \in \mathbb{R}^{128 \times 128}$ is the degraded PAN image, $S_PAN \in \mathbb{R}^{128 \times 128}$ is the small-size PAN images, $L_PAN \in \mathbb{R}^{256 \times 256}$ is the large-size PAN images; (b) Resized MS images (c) Outputs of our MBPRR-Net model.

3) *CC*: CC is defined as characterizes of geometric distortion which can be computed as follows:

$$\text{CC} = \frac{1}{c} \sum_{i=1}^c \frac{\sum_{j=1}^n (\hat{y}_j^i - \mu_{\hat{y}^i})(y_j^i - \mu_{y^i})}{\sqrt{\sum_{j=1}^n (\hat{y}_j^i - \mu_{\hat{y}^i})^2 \sum_{j=1}^n (y_j^i - \mu_{y^i})^2}}, \quad (11)$$

where μ is the mean value of image. The closer CC to 1, the more correlated the two images are.

4) *UIQI*: UIQI considers correlation loss, brightness distortion, and contrast distortion. UIQI is formulated as follows:

$$\text{UIQI} = \frac{\sigma_{\hat{y}y}}{\sigma_{\hat{y}}\sigma_y} \frac{2\mu_{\hat{y}}\mu_y}{\mu_{\hat{y}}^2 + \mu_y^2} \frac{2\sigma_{\hat{y}}\sigma_y}{\sigma_{\hat{y}}^2 + \sigma_y^2}, \quad (12)$$

5) *SAM*: In an image, SAM employ a vector to represent the spectrum of each pixel. SAM is used to represent the similarity between two spectra, and utilizes the angle between two spectral vectors to calculate the similarity. Note that the SAM is smaller, the angle of two spectral vectors is smaller, and the higher the degree of similarity between the two spectra.

$$\text{SAM} = \cos^{-1}\left(\frac{\hat{y}^T y}{\sqrt{\hat{y}^T \hat{y}} \sqrt{y^T y}}\right), \quad (13)$$

C. Experimental Comparison and Discussions

In this section, we analyze the experimental results of our method, and compare with some exiting colorization and super-resolution methods in terms of objective data and subjective vision.

First, we evaluate the model performance under different types of input images, we show four groups of model outputs

in Fig. 7 when input different kind of images, the input images including three types: the degraded PAN images ($D_PAN \in \mathbb{R}^{128 \times 128}$), the small-size PAN images ($S_PAN \in \mathbb{R}^{128 \times 128}$), and the large-size PAN images ($L_PAN \in \mathbb{R}^{256 \times 256}$). From Fig. 7, we can see that the output images have higher spatial resolution than the input PAN images, and have color information. In general, the model can generate near realistic images for any size input images.

TABLE II: Quantitative results of the PAN image super-resolution task, red text marks the best performance.

Method	PSNR (↑)	CC (↑)	UIQI (↑)	SAM (↓)
SRCNN [8]	37.02	0.983	0.982	0.049
SRGAN [13]	36.74	0.982	0.981	0.051
EDSR [32]	37.85	0.984	0.983	0.044
LapSR [42]	36.14	0.976	0.975	0.055
DRN [34]	30.30	0.923	0.899	0.111
MHAN [43]	38.27	0.984	0.984	0.044
Ours	38.34	0.985	0.984	0.043

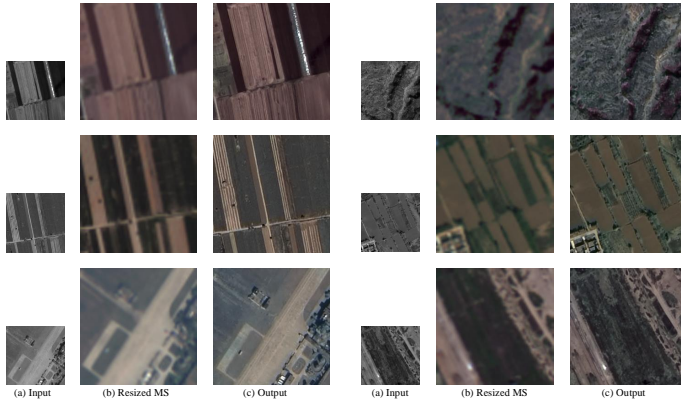


Fig. 8: Experimental results on land scenes. (a) Input; (b) Resized MS image; (c) Output.

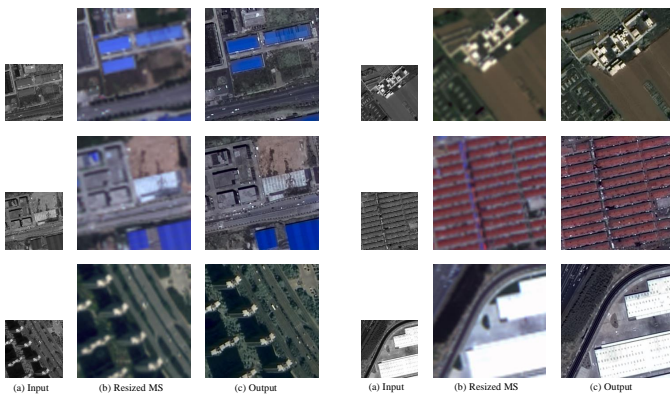


Fig. 9: Experimental results on building scenes. (a) Input; (b) Resized MS image; (c) Output.

Second, we show the experimental results by category in Fig. 8 to Fig. 11, mainly showing land, building, river and other categories that are not easy to classify. Experiments show that the results of our model can improve the spatial resolution

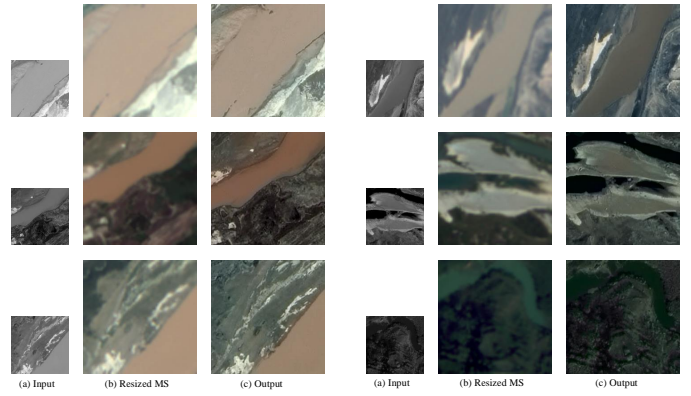


Fig. 10: Experimental results on river scenes. (a) Input; (b) Resized MS image; (c) Output.

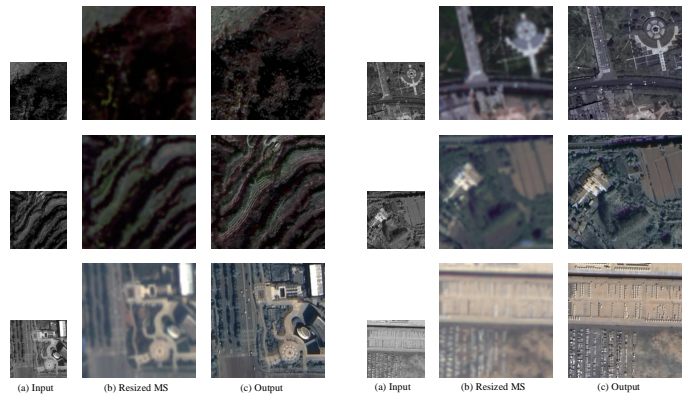


Fig. 11: Experimental results on some scenes that are not easy to classify. (a) Input image; (b) Resized MS image; (c) Output image.

(the MBPRR-Net model's output image is wider and higher than the MBPRR-Net model's input image), and also improve the spectral resolution (the color information of the MBPRR-Net model's output image is same as the MS image). Fig. 8 to Fig. 11 show that our output image has no artifacts or blurred edges, which illustrates that our model is successful in restoring the spatial resolution. Fig. 8 to Fig. 10 show that our model successfully solves the problem of large intra-class differences in remote sensing images. For the same kind of objects, our model can recover different spectral or color information according to MS images. For example, the land in Fig. 8 is brownish-yellow, green or gray, and the building in Fig. 9 is blue, silver, white, or dark gray, and the river in Fig. 10 is blackish green, green or brownish-yellow. Our model also solves the problem of small inter-class differences in remote sensing images. For example, the land in Fig. 8 appears brownish-yellow, and the river in Fig. 10 also appears brownish-yellow, which realizes the reconstruction of the same spectral or color information for different types of objects.

Third, we compare the effect of the MBPRR-Net model with some excellent super-resolution models including SRCNN [8], SRGAN [13], EDSR [32], LapSR [42], DRN [34] and MHAN [43]. The results of different methods are shown in Fig. 12. The output images produced by our method are comparable

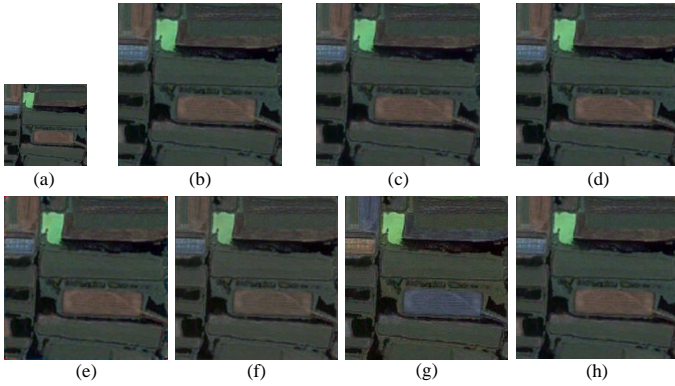


Fig. 12: Image super-resolution results of our MBPRR-Net and comparison algorithm. (a) Input; (b) SRCNN [8]; (c) SRGAN [13]; (d) EDSR [32]; (e) LapSR [42]; (f) DRN [34]; (g) MHAN [43]; (h) Ours.

to the image generated by other super-resolution methods, visually. In particular, our method does not produce noticeable forged artifacts. The experiment result shows that our method has higher value in objective indicators than other methods, which further illustrates the effectiveness of our MBPRR-Net model.

TABLE III: Quantitative results of the PAN image colorization task, red text marks the best performance.

Method	PSNR (\uparrow)	CC (\uparrow)	UIQI (\uparrow)	SAM (\downarrow)
Iizuka [22]	35.38	0.977	0.975	0.061
Zhang [23]	34.06	0.969	0.966	0.073
Isola [26]	33.90	0.970	0.966	0.075
Yoo [27]	32.71	0.968	0.963	0.085
Vitoria [28]	35.02	0.975	0.973	0.064
Ours	36.06	0.979	0.977	0.056

Fourth, we compare our method with other excellent colorization models. All the colorization models use the same input features, these models are trained with the same iterations. The colorization visual results of PAN image of our algorithm (in Section. III) and the comparison algorithms (Iizuka [22], Zhang [23], Isola [26], Yoo [27], Vitoria [28]) in Dataset-I are shown in Fig. 13. Fig. 13 (a) is MS image $\in \mathbb{R}^{C \times 64 \times 64}$, for visual contrast the size of MS image is enlarged to 256×256 . Red rectangular boxes are used to mark some small areas where the color detail is significantly incorrect compared to our method. We can observe that: 1) Our proposed method can generate a image with color information that is closer to MS image than other methods. For example, the 1st row of Fig. 13 shows that our method can colorize the roof, land, and vegetation correctly, while other methods have some wrong colors (i.e., the roof in the upper left corner is gray whereas in the MS image it is blue, the land in the red rectangular box is green whereas in the MS image it is brown). 2) Our model is especially good at colorizing rare instances. For example, in the 4th row, the MS image has a green plant in the red box, and only our method colorizes the plant green whereas all other methods colorize the plant

TABLE IV: Quantitative results of our model, colorization and SR combined models (first use SR model then use colorization model)

SR	Colorization	PSNR (\uparrow)	CC (\uparrow)	UIOI (\uparrow)	SAM (\downarrow)
SRGAN [13]	Iizuka [22]	23.63	0.754	0.646	0.208
	Yoo [27]	32.68	0.869	0.859	0.082
	Zhang [23]	31.97	0.784	0.775	0.089
	Vitoria [28]	30.56	0.760	0.761	0.127
	Isola [26]	30.75	0.933	0.925	0.110
LAPSR [42]	Iizuka [22]	28.78	0.956	0.937	0.086
	Yoo [27]	33.26	0.959	0.955	0.089
	Zhang [23]	31.30	0.960	0.947	0.106
	Vitoria [28]	32.74	0.941	0.935	0.102
	Isola [26]	32.27	0.954	0.949	0.090
EDSR [32]	Iizuka [22]	29.37	0.961	0.943	0.081
	Yoo [27]	33.01	0.958	0.953	0.089
	Zhang [23]	31.97	0.955	0.948	0.101
	Vitoria [28]	32.88	0.957	0.952	0.091
	Isola [26]	32.63	0.957	0.953	0.087
MHAN [43]	Iizuka [22]	29.26	0.960	0.942	0.083
	Yoo [27]	33.00	0.959	0.954	0.090
	Zhang [23]	33.73	0.960	0.956	0.083
	Vitoria [28]	29.06	0.939	0.927	0.099
	Isola [26]	32.44	0.957	0.952	0.089
SRCNN [8]	Iizuka [22]	29.11	0.959	0.942	0.083
	Yoo [27]	33.41	0.959	0.955	0.087
	Zhang [23]	28.60	0.954	0.937	0.092
	Vitoria [28]	28.88	0.941	0.928	0.098
	Isola [26]	32.41	0.956	0.951	0.089
DRN [34]	Iizuka [22]	32.25	0.923	0.897	0.133
	Yoo [27]	31.35	0.910	0.893	0.152
	Zhang [23]	31.50	0.921	0.905	0.140
	Vitoria [28]	31.25	0.912	0.894	0.155
	Isola [26]	20.17	0.715	0.608	0.221
Our		33.87	0.963	0.961	0.072

brown. 3) Our method does not have the problem of color overflow. For example, in the last row, the road in Fig. 13 (d) appears blue, the road in Fig. 13 (f) and (g) appear green, but blue and green are both colors that should not be on the road. However, our method gives the road normal color which is same as the MS image. In addition to visual analysis, we also evaluate colorization quality quantitatively. We present the average evaluation metrics on the testing dataset in Table III. According to the above analysis, we can infer that the proposed method is better than the compared algorithms both visual effect and objective evaluation metrics.

Fifth, we combine SR models and colorization models to compare with our model. Table V and Table IV show the quantitative results of two groups of comparative experiments respectively. By comparing V and Table IV, it can be seen that the effect of our model is better than the combination of SR model and colorization model. At the same time, it is not difficult to see that the result of using SR model first and then colorization model is better than that of using colorization model first and then SR model on the whole, which indicates that the sequence of models will affect the final experimental results. However, our model doesn't have the problem of sequencing because we use one model to achieve the effect of SR and colorization models at the same time. Therefore,

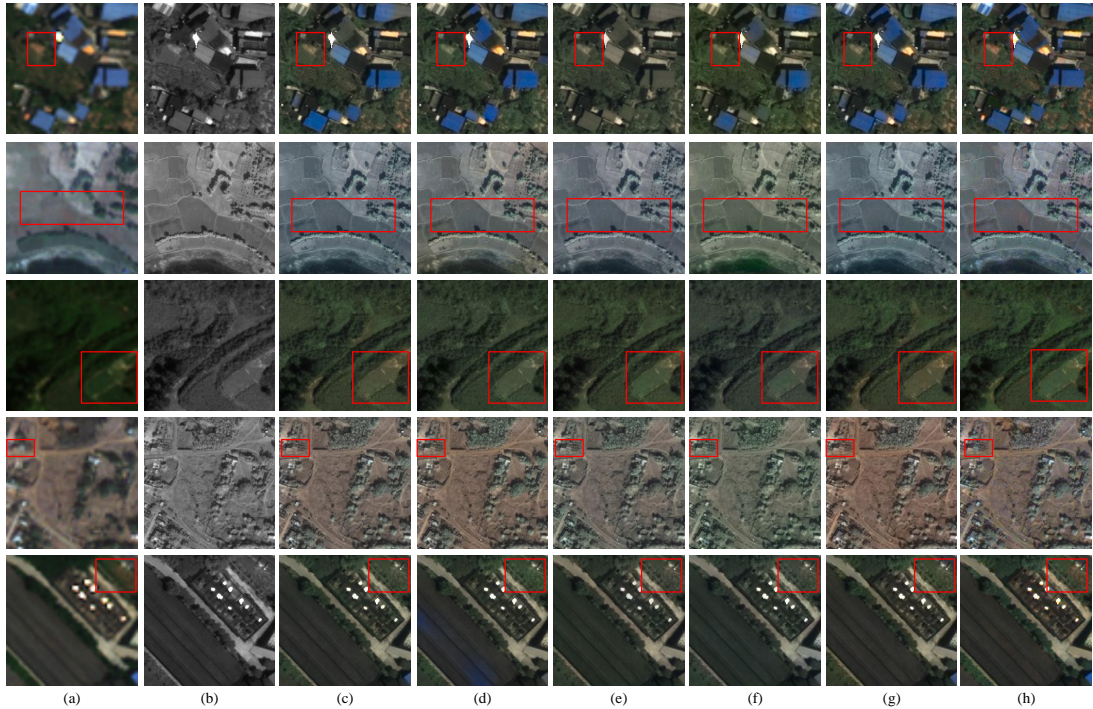


Fig. 13: Colorization results of our MBPRR-Net and comparison algorithm. (a) Resized MS image; (b) PAN image; (c) Iizuka [22]; (d) Zhang [23]; (e) Isola [26]; (f) Yoo [27]; (g) Vitoria [28]; (h) Ours.

our model not only has the best experimental effect, but also does not need to consider the order of the SR model and colorization model, which can be implemented in one step.

Finally, we compared our method with the pan-sharpening model, the experimental results of the Z-PNN model proposed by Ciotola et al. [44], the PanNet model proposed by Yang et al. [45] and the ZeRGAN model proposed by Diao et al. [46] are shown in Fig. 14. The pan-sharpening model requires two inputs, MS and PAN, while our model requires only one input. It can be seen from Fig. 14 that the spectral information of the images output by PNN and PanNet models is rich, but it is obviously inconsistent with the spectral information of MS, that is, these two models can restore the spectrum, but the restored spectrum does not conform to the real situation. Compared with the ZeRGAN model, the output images of our model have clear texture, and the spectral information is closer to MS.

Thus, we can infer that the proposed method is better than the compared algorithms both visual effect and objective evaluation metrics.

D. Ablation Study

To determine the appropriate number of branches of MBPRR-Net and prove the effectiveness of modules in MBPRR-Net, we performed two ablation experiments respectively.

1) *Selection of branch number*: To determine the number of branches of our MBPRR-Net model, we experimented with single branch, two branches, three branches, four branches, and five branches. It can be seen from Table VI that the

performance of MBPRR-Net is the best when four branches are used. There are three possible reasons why using four branches performs well. First, PAN image has the problem of large differences between same class and small differences between different classes. This problem can be solved by designing a module to extract more useful features. Using multiple branches is helpful to extract more useful features from the input image. Therefore, it is possible to adopt a model with four branches will be better than a model with single branch, two branches or three branch. Second, the fewer branches are used, the fewer feature maps can be used for aggregation. The feature aggregation module can use the extracted feature map to make the aggregated feature map wider and higher, so that the extracted features can be fully utilized to reconstruct an image. Therefore, there are more branches will help the model improve the performance of the aggregation module. Third, the effect of the MBPRR-Net does not always increase with the increase of the number of branches, that is, when the number of branches increases to a certain extent and then continues to increase, the effect of the MBPRR-Net decreases. This is because the number of branches increases, the depth of the model will increase, and may cause vanishing gradient problem. At the same time, the width and height of the extracted feature map will become smaller, while the too small feature map has little useful information. Therefore, the back branches can not improve the effect of the MBPRR-Net. Through experiments, we find that MBPRR-Net has the best effect when the number of branches is four.

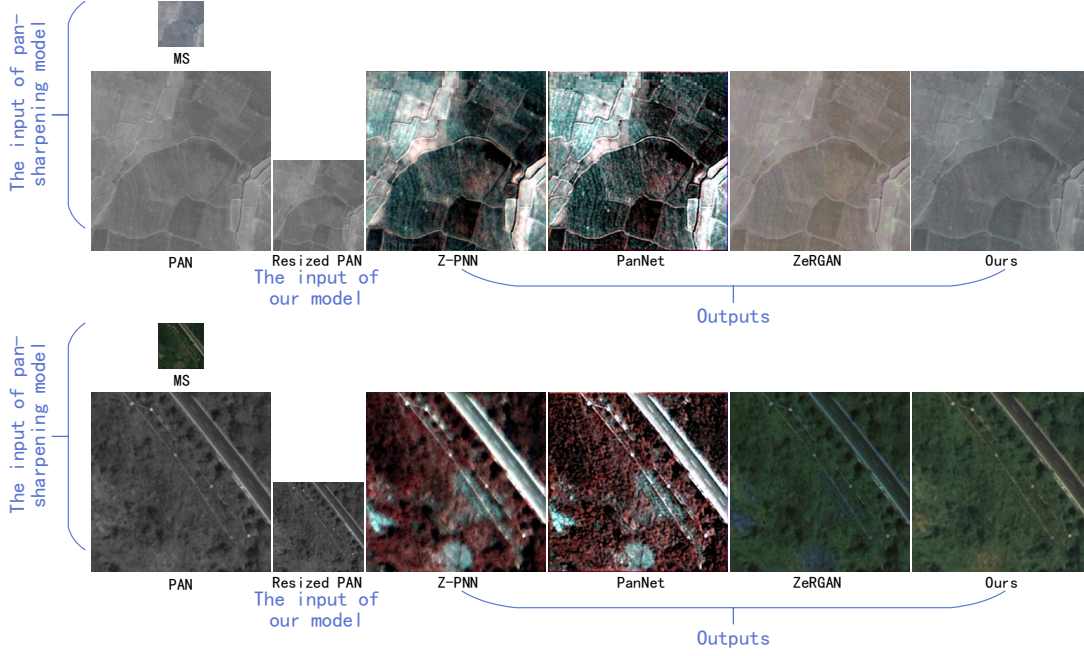


Fig. 14: Results of our MBPRR-Net and pan-sharpening algorithm.

TABLE V: Quantitative results of our model, colorization and SR combined models (first use colorization model then use SR model).

Colorization	SR	PSNR (↑)	CC (↑)	UIOI (↑)	SAM (↓)
Iizuka [22]	SRCNN [8]	32.15	0.951	0.948	0.088
	SRGAN [13]	30.54	0.900	0.848	0.076
	LAPSR [42]	31.58	0.944	0.941	0.093
	EDSR [32]	32.30	0.951	0.949	0.087
	DRN [34]	28.40	0.942	0.927	0.103
	MHAN [43]	29.10	0.917	0.821	0.080
Yoo [27]	SRCNN [8]	31.56	0.951	0.947	0.094
	SRGAN [13]	26.50	0.937	0.770	0.160
	LAPSR [42]	31.41	0.949	0.945	0.097
	EDSR [32]	31.39	0.948	0.944	0.096
	DRN [34]	26.18	0.843	0.832	0.162
	MHAN [43]	24.92	0.805	0.556	0.217
Zhang [23]	SRCNN [8]	30.10	0.953	0.941	0.110
	SRGAN [13]	27.49	0.937	0.811	0.150
	LAPSR [42]	29.76	0.947	0.935	0.113
	EDSR [32]	30.32	0.955	0.943	0.108
	DRN [34]	28.59	0.940	0.927	0.107
	MHAN [43]	24.94	0.880	0.588	0.214
Vitoria [28]	SRCNN [8]	32.65	0.958	0.955	0.083
	SRGAN [13]	27.34	0.915	0.783	0.153
	LAPSR [42]	32.24	0.951	0.948	0.086
	EDSR [32]	33.26	0.959	0.957	0.077
	DRN [34]	29.05	0.945	0.933	0.098
	MHAN [43]	25.10	0.805	0.562	0.212
Isola [26]	SRCNN [8]	32.49	0.955	0.952	0.087
	SRGAN [13]	27.16	0.917	0.769	0.155
	LAPSR [42]	32.03	0.950	0.946	0.092
	EDSR [32]	32.74	0.957	0.953	0.085
	DRN [34]	28.49	0.939	0.925	0.108
	MHAN [43]	24.86	0.786	0.539	0.216
Our		33.87	0.963	0.961	0.072

TABLE VI: An ablation study on the number of effective branches, red text marks the best performance.

Branch number	PSNR (↑)	CC (↑)	UIQI (↑)	SAM (↓)
1	27.33	0.836	0.828	0.154
2	33.41	0.961	0.959	0.076
3	33.75	0.962	0.960	0.072
5	33.74	0.962	0.960	0.071
4 (Our)	33.87	0.963	0.961	0.072

TABLE VII: An ablation study on different combinations of FCMB, Cubic and SCB, red text marks the best performance.

	1	2	3	4	5	6	7	8
FCMB	✗	✓	✗	✗	✓	✓	✗	✓
Cubic	✗	✗	✓	✗	✓	✗	✓	✓
SCB	✗	✗	✗	✓	✗	✓	✓	✓
PSNR	33.67	33.75	33.85	27.35	33.78	33.78	33.65	33.87

2) *Effectiveness of modules in MBPRR-Net:* To validate the effect of several important modules in our MBPRR-Net model, we do an ablation study by combining different modules. The average PSNR of different combinations is illustrated in Table VII. First, we can see that the performance of the baseline without FCMB, Cubic, and SCB is not very well (PSNR = 33.67 dB) from 1st group in Table VII. Second, we add one of FCMB, Cubic, and SCB to the baseline, respectively (from 2nd to 4th groups in Table VII). We can validate that add each module to the baseline can improve the effect of the baseline except add SCB to the baseline. This is because the SCB module is used for feature recovery, which is based on the condition that abundant features are extracted. Thus, the SCB module would not be able to perform its function without the

FCMB module to extract features and cubic filter to enhance features. Then, we add two modules to the baseline (from 5th to 7th groups in Table VII). By comparing the 4th and 6th groups, we can see that using both SCB module and FCMB module is better than using only SCB module. Since Cubic performs well (PSNR = 33.85dB), the model with FCMB and SCB also performs well (PSNR = 33.78 dB). Finally, we combine these three modules together to get the 8th group in Table VII, and three components perform the best (PSNR = 33.87dB). These quantitative analyses show that our proposed FCMB, Cubic, and SCB modules are useful.

V. CONCLUSION

In this paper, we propose a novel model named MBPRR-Net to restore the spatial and spectral resolution of PAN image simultaneously. To exploit the correlation between the feature channels, we design a module FCMB to fuse neighboring features in channel dimension. We use a multi-branch structure to obtain the features in different scales, then we aggregate the features of each branch by pixel shuffling to make full use of the features extracted by each branch. We use Cubic filter to weight the extracted features according to their importance. At the same time, we add an attention mechanism to the SCB module to assign weights to the features to be recovered so that the important information will not be ignored. To recover the spatial resolution and spectral resolution, we use two branches to generate the L channel and ab channel of the image respectively. We verified the spectral resolution improvement by comparing with the colorized model, the spatial resolution improvement by comparing with the super-resolution model. Extensive experiments and visualization demonstrate that our MBPRR-Net outperforms most existing colorization and super-resolution methods.

Since our model needs to improve the spatial and spectral resolution of remote sensing images at the same time, it is more complex than the super-resolution model that only improves the spatial resolution and the colorization model that only improves the spectral resolution. In the future, we will optimize the model and speed up the training and inference speed without reducing the effect of the model.

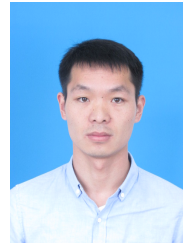
CONFLICT OF INTEREST

The authors declare no conflict of interest.

REFERENCES

- [1] H. Li, R. Li, Y. Yang, B. Cao, Z. Bian, T. Hu, Y. Du, L. Sun, and Q. Liu, "Temperature-based and radiance-based validation of the collection 6 myd11 and myd21 land surface temperature products over barren surfaces in northwestern china," *IEEE Transactions on Geoscience and Remote Sensing*, vol. 59, no. 2, pp. 1794–1807, 2021.
- [2] L. Jiao, L. Huo, C. Hu, and P. Tang, "Refined unet v3: Efficient end-to-end patch-wise network for cloud and shadow segmentation with multi-channel spectral features," *Neural Networks*, vol. 143, pp. 767–782, 2021. [Online]. Available: <https://www.sciencedirect.com/science/article/pii/S0893608021003130>
- [3] A. Sharma, X. Liu, and X. Yang, "Land cover classification from multi-temporal, multi-spectral remotely sensed imagery using patch-based recurrent neural networks," *Neural Networks*, vol. 105, pp. 346–355, 2018. [Online]. Available: <https://www.sciencedirect.com/science/article/pii/S0893608018301813>
- [4] M. G. Gale, G. J. Cary, A. I. Van Dijk, and M. Yebra, "Forest fire fuel through the lens of remote sensing: Review of approaches, challenges and future directions in the remote sensing of biotic determinants of fire behaviour," *Remote Sensing of Environment*, vol. 255, p. 112282, 2021. [Online]. Available: <https://www.sciencedirect.com/science/article/pii/S0034425720306556>
- [5] K. Indrajit and R. Moumita, "Deep neural network-based heterogeneous domain adaptation using ensemble decision making in land cover classification," *IEEE Transactions on Artificial Intelligence*, vol. 1, no. 2, pp. 167–180, 2020.
- [6] A. Sharma, X. Liu, X. Yang, and D. Shi, "A patch-based convolutional neural network for remote sensing image classification," *Neural Networks*, vol. 95, pp. 19–28, 2017. [Online]. Available: <https://www.sciencedirect.com/science/article/pii/S0893608017301806>
- [7] H. Hosseinpour, F. Samadzadegan, and F. D. Javan, "Cmgfnet: A deep cross-modal gated fusion network for building extraction from very high-resolution remote sensing images," *ISPRS Journal of Photogrammetry and Remote Sensing*, vol. 184, pp. 96–115, 2022. [Online]. Available: <https://www.sciencedirect.com/science/article/pii/S0924271621003294>
- [8] C. Dong, C. C. Loy, K. He, and X. Tang, "Image super-resolution using deep convolutional networks," *IEEE Transactions on Pattern Analysis and Machine Intelligence*, vol. 38, no. 2, pp. 295–307, 2016.
- [9] C. Dong, C. C. Loy, and X. Tang, "Accelerating the super-resolution convolutional neural network," in *Computer Vision – ECCV 2016*, B. Leibe, J. Matas, N. Sebe, and M. Welling, Eds. Cham: Springer International Publishing, 2016, pp. 391–407.
- [10] Y. Zhang, K. Li, K. Li, L. Wang, B. Zhong, and Y. Fu, "Image super-resolution using very deep residual channel attention networks," in *Computer Vision – ECCV 2018*, V. Ferrari, M. Hebert, C. Sminchisescu, and Y. Weiss, Eds. Cham: Springer International Publishing, 2018, pp. 294–310.
- [11] K. Jiang, Z. Wang, P. Yi, and J. Jiang, "Hierarchical dense recursive network for image super-resolution," *Pattern Recognition*, vol. 107, p. 107475, 2020. [Online]. Available: <https://www.sciencedirect.com/science/article/pii/S0031320320302788>
- [12] Y. Mei, Y. Fan, Y. Zhou, L. Huang, T. S. Huang, and H. Shi, "Image super-resolution with cross-scale non-local attention and exhaustive self-exemplars mining," in *2020 IEEE/CVF Conference on Computer Vision and Pattern Recognition (CVPR)*, 2020, pp. 5689–5698.
- [13] C. Ledig, L. Theis, F. Husz, J. Caballero, A. Cunningham, A. Acosta, A. Aitken, A. Tejani, J. Totz, Z. Wang, and W. Shi, "Photo-realistic single image super-resolution using a generative adversarial network," in *2017 IEEE Conference on Computer Vision and Pattern Recognition (CVPR)*, 2017, pp. 105–114.
- [14] N. Anagnostopoulos, C. Iakovidou, A. Amanatiadis, Y. Boutalis, and S. A. Chatzichristofis, "Two-staged image colorization based on salient contours," in *2014 IEEE International Conference on Imaging Systems and Techniques (IST) Proceedings*, 2014, pp. 381–385.
- [15] P. Sangkloy, J. Lu, C. Fang, F. Yu, and J. Hays, "Scribbler: Controlling deep image synthesis with sketch and color," in *2017 IEEE Conference on Computer Vision and Pattern Recognition (CVPR)*, 2017, pp. 6836–6845.
- [16] Y. Ci, X. Ma, Z. Wang, H. Li, and Z. Luo, "User-guided deep anime line art colorization with conditional adversarial networks," in *Proceedings of the 26th ACM International Conference on Multimedia*. New York, NY, USA: Association for Computing Machinery, 2018, pp. 1536–1544. [Online]. Available: <https://doi.org/10.1145/3240508.3240661>
- [17] A. Y.-S. Chia, S. Zhuo, R. K. Gupta, Y.-W. Tai, S.-Y. Cho, P. Tan, and S. Lin, "Semantic colorization with internet images," *ACM Trans. Graph.*, vol. 30, no. 6, pp. 1–8, Dec. 2011. [Online]. Available: <https://doi.org/10.1145/2070781.2024190>
- [18] M. He, D. Chen, J. Liao, P. V. Sander, and L. Yuan, "Deep exemplar-based colorization," *ACM Trans. Graph.*, vol. 37, no. 4, Jul. 2018. [Online]. Available: <https://doi.org/10.1145/3197517.3201365>
- [19] J. Lee, E. Kim, Y. Lee, D. Kim, J. Chang, and J. Choo, "Reference-based sketch image colorization using augmented-self reference and dense semantic correspondence," in *2020 IEEE/CVF Conference on Computer Vision and Pattern Recognition (CVPR)*, 2020, pp. 5800–5809.
- [20] H. Bahng, S. Yoo, W. Cho, D. K. Park, Z. Wu, X. Ma, and J. Choo, "Coloring with words: Guiding image colorization through text-based palette generation," in *Computer Vision – ECCV 2018*, V. Ferrari, M. Hebert, C. Sminchisescu, and Y. Weiss, Eds. Cham: Springer International Publishing, 2018, pp. 443–459.
- [21] H. Kim, H. Y. Jhoo, E. Park, and S. Yoo, "Tag2pix: Line art colorization using text tag with secant and changing loss," in *2019 IEEE/CVF International Conference on Computer Vision (ICCV)*, 2019, pp. 9055–9064.

- [22] S. Iizuka, E. Simo-Serra, and H. Ishikawa, "Let there be color! joint end-to-end learning of global and local image priors for automatic image colorization with simultaneous classification," *ACM Trans. Graph.*, vol. 35, no. 4, Jul. 2016. [Online]. Available: <https://doi.org/10.1145/2897824.2925974>
- [23] R. Zhang, P. Isola, and A. A. Efros, "Colorful image colorization," in *Computer Vision – ECCV 2016*, B. Leibe, J. Matas, N. Sebe, and M. Welling, Eds. Cham: Springer International Publishing, 2016, pp. 649–666.
- [24] G. Özbulak, "Image colorization by capsule networks," in *2019 IEEE/CVF Conference on Computer Vision and Pattern Recognition Workshops (CVPRW)*, 2019, pp. 2150–2158.
- [25] J.-W. Su, H.-K. Chu, and J.-B. Huang, "Instance-aware image colorization," in *2020 IEEE/CVF Conference on Computer Vision and Pattern Recognition (CVPR)*, 2020, pp. 7965–7974.
- [26] P. Isola, J.-Y. Zhu, T. Zhou, and A. A. Efros, "Image-to-image translation with conditional adversarial networks," in *2017 IEEE Conference on Computer Vision and Pattern Recognition (CVPR)*, 2017, pp. 5967–5976.
- [27] S. Yoo, H. Bahng, S. Chung, J. Lee, J. Chang, and J. Choo, "Coloring with limited data: Few-shot colorization via memory augmented networks," in *2019 IEEE/CVF Conference on Computer Vision and Pattern Recognition (CVPR)*, 2019, pp. 11 275–11 284.
- [28] P. Vitoria, L. Raad, and C. Ballester, "Chromagan: Adversarial picture colorization with semantic class distribution," in *2020 IEEE Winter Conference on Applications of Computer Vision (WACV)*, 2020, pp. 2434–2443.
- [29] G. Ji, Z. Wang, L. Zhou, Y. Xia, S. Zhong, and S. Gong, "Sar image colorization using multidomain cycle-consistency generative adversarial network," *IEEE Geoscience and Remote Sensing Letters*, vol. 18, no. 2, pp. 296–300, 2021.
- [30] F. Ozcelik, U. Alganci, E. Sertel, and G. Unal, "Rethinking cnn-based pansharpening: Guided colorization of panchromatic images via gans," *IEEE Transactions on Geoscience and Remote Sensing*, vol. 59, no. 4, pp. 3486–3501, 2021.
- [31] X. Lu, J. Zhang, D. Yang, L. Xu, and F. Jia, "Cascaded convolutional neural network-based hyperspectral image resolution enhancement via an auxiliary panchromatic image," *IEEE Transactions on Image Processing*, vol. 30, pp. 6815–6828, 2021.
- [32] B. Lim, S. Son, H. Kim, S. Nah, and K. M. Lee, "Enhanced deep residual networks for single image super-resolution," in *2017 IEEE Conference on Computer Vision and Pattern Recognition Workshops (CVPRW)*, 2017, pp. 1132–1140.
- [33] K. He, X. Zhang, S. Ren, and J. Sun, "Deep residual learning for image recognition," in *2016 IEEE Conference on Computer Vision and Pattern Recognition (CVPR)*, 2016, pp. 770–778.
- [34] Y. Guo, J. Chen, J. Wang, Q. Chen, J. Cao, Z. Deng, Y. Xu, and M. Tan, "Closed-loop matters: Dual regression networks for single image super-resolution," in *2020 IEEE/CVF Conference on Computer Vision and Pattern Recognition (CVPR)*, 2020, pp. 5406–5415.
- [35] K. Simonyan and A. Zisserman, "Very deep convolutional networks for large-scale image recognition," *Computer Science*, 2014.
- [36] J. An, K. G. Kpeyton, and Q. Shi, "Grayscale images colorization with convolutional neural networks," *Soft Computing*, vol. 24, no. 3, pp. 4751–4758, 2020. [Online]. Available: <https://doi.org/10.1007/s00500-020-04711-3>
- [37] S. Liu, D. Huang, and Y. Wang, "Receptive field block net for accurate and fast object detection," in *Computer Vision – ECCV 2018*, V. Ferrari, M. Hebert, C. Sminchisescu, and Y. Weiss, Eds. Cham: Springer International Publishing, 2018, pp. 404–419.
- [38] D. Li, J. Hu, C. Wang, X. Li, Q. She, L. Zhu, T. Zhang, and Q. Chen, "Involution: Inverting the inheritance of convolution for visual recognition," 2021.
- [39] H. Jie, S. Li, S. Gang, and S. Albanie, "Squeeze-and-excitation networks," *IEEE Transactions on Pattern Analysis and Machine Intelligence*, vol. PP, no. 99, 2017.
- [40] S. Moran, P. Marza, S. McDonagh, S. Parisot, and G. Slabaugh, "Deepplpf: Deep local parametric filters for image enhancement," in *2020 IEEE/CVF Conference on Computer Vision and Pattern Recognition (CVPR)*, 2020.
- [41] D. Misra, "Mish: A self regularized non-monotonic neural activation function," *CoRR*, vol. abs/1908.08681, 2019. [Online]. Available: <http://arxiv.org/abs/1908.08681>
- [42] W.-S. Lai, J.-B. Huang, N. Ahuja, and M.-H. Yang, "Deep laplacian pyramid networks for fast and accurate super-resolution," in *2017 IEEE Conference on Computer Vision and Pattern Recognition (CVPR)*, 2017, pp. 5835–5843.
- [43] D. Zhang, J. Shao, X. Li, and H. T. Shen, "Remote sensing image super-resolution via mixed high-order attention network," *IEEE Transactions on Geoscience and Remote Sensing*, vol. 59, no. 6, pp. 5183–5196, 2021.
- [44] M. Ciotola, S. Vitale, A. Mazza, G. Poggi, and G. Scarpa, "Pansharpening by convolutional neural networks in the full resolution framework," *IEEE Transactions on Geoscience and Remote Sensing*, vol. 60, pp. 1–17, 2022.
- [45] J. Yang, X. Fu, Y. Hu, Y. Huang, X. Ding, and J. Paisley, "Pannet: A deep network architecture for pan-sharpening," in *Proceedings of the IEEE international conference on computer vision*, 2017, pp. 5449–5457.
- [46] W. Diao, F. Zhang, J. Sun, Y. Xing, K. Zhang, and L. Bruzzone, "Zergan: Zero-reference gan for fusion of multispectral and panchromatic images," *IEEE Transactions on Neural Networks and Learning Systems*, 2022.



optimization algorithm, and fuzzy set theory.



Xin Jin received the B.S. degree in electronics and information engineering from Henan Normal University, Xinxiang, China, in 2013, and the Ph.D. degree in communication and information systems from Yunnan University, Kunming, China, in 2018. He was a Post-Doctoral Fellow with the School of Software, Yunnan University from 2018 to 2020. He is an Associate Professor with the School of Software, Yunnan University. His research interests include pulse coupled neural networks and its applications, image processing, information fusion, optimization algorithm, and fuzzy set theory.



Ling Liu is a master degree candidate at the School of Software, Yunnan University, Kunming, China. She received her BE degree in software engineering from the Yunnan University in 2019. Her research interests include deep neural networks, image colorization, and image super-resolution.



Xiaoxuan Ren received the B.E. degree in computer science and technology from Beijing Jiaotong University in 2021. She is pursuing the master's degree with the School of Software, Yunnan University. Her current research interests include image processing, deep learning and image super-resolution.

include deep neural networks, fuzzy set theory, bio-informatics, image processing, and information fusion.



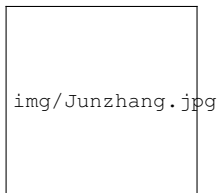
Qian Jiang received the B.S. degree in thermal energy and power engineering and the M.S. degree in power engineering and engineering thermo-physics from Central South University (CSU), Changsha, China, in 2012 and 2015, respectively, and the Ph.D. degree in communication and information systems from Yunnan University, Kunming, China, in 2019. She was a Post-Doctoral Fellow with the School of Software, Yunnan University from 2019 to 2021. She is an Associate Professor with the School of Software, Yunnan University. Her research interests

include deep neural networks, fuzzy set theory, bio-informatics, image processing, and information fusion.

Shinje Lee received the M.Sc. (Eng) degree from the Department of Computer Science, The University of Sheffield, Sheffield, U.K., in 2001, the M.Phil. degree from the Judge Business School, University of Cambridge, Cambridge, U.K., in 2012, and the Ph.D. degree from the School of Computer Science, The University of Manchester, Manchester, U.K., in 2011. He is currently an Associate Professor with National Chiao Tung University, Hsinchu, Taiwan. He also made his academic career in Poland and Taiwan successively. In addition, he also had practical experiences at Fujitsu (Taipei Branch) and Microsoft (Taipei Branch)

from 2002 to 2005. Furthermore, his research interests primarily comprise machine learning, computational intelligence and decision support system, operational research, and technology policy, especially for the climate change issues and energy prediction.

Jun Zhang received the MS.D. degree from School of Software, Yunnan University, Kunming, China.



Shaowen Yao is a Professor at the School of Software, Yunnan University, China. He received his BS and MS degrees in telecommunication engineering from the Yunnan University in 1988 and 1991, respectively, and his PhD degree in computer application technology from University of Electronic Science and Technology of China (UESTC) in 2002. His current research interests include neural network theory and applications, cloud computing and big data computing.